ERDC/GSL TR-13-5

US Army Corps
of Engineers®
Engineer Research and
Development Center

ERDC
INNOVATIVE SOLUTIONS
for a safer, better world

A Computational Model to Simulate Groundwater Seepage Risk in Support of Geotechnical Investigations of Levee and Dam Projects

Brendan T. Yuill and Carla M. Roig-Silva

March 2013

Geotechnical and Structures Laboratory

The US Army Engineer Research and Development Center (ERDC) solves the nation's toughest engineering and environmental challenges. ERDC develops innovative solutions in civil and military engineering, geospatial sciences, water resources, and environmental sciences for the Army, the Department of Defense, civilian agencies, and our nation's public good. Find out more at www.erdc.usace.army.mil.

To search for other technical reports published by ERDC, visit the ERDC online library at http://acwc.sdp.sirsi.net/client/default.

ERDC/GSL TR-13-5
March 2013

A Computational Model to Simulate Groundwater Seepage Risk in Support of Geotechnical Investigations of Levee and Dam Projects

Brendan T. Yuill and Carla M. Roig-Silva

Geotechnical and Structures Laboratory
US Army Engineer Research and Development Center
3909 Halls Ferry Road
Vicksburg, MS 39180-6199

Final report

Prepared for US Army Corps of Engineers, Fort Worth District
809 Taylor Street 4A01
Fort Worth, TX 76102

Abstract

The amount and distribution of coarse-grained sediment relative to fine-grained sediment within a floodplain influences the floodplain's geotechnical properties, including the potential for groundwater seepage. Seepage is a primary driver of levee and dam failure, and understanding it is of paramount concern to water resource engineers and managers. This report documents the results of a computational modeling study that simulated alluvial floodplain construction by using simple geomorphic process-imitating rules. The model aggrades an alluvial floodplain, creating floodplain architecture by differentiating between sediment deposited by channel processes (coarse sediment) and sediment deposited by overbank flood processes (fine sediment). The evolution of two floodplain cross sections of the Trinity River near Dallas, Texas, is simulated under five scenarios. The study area is the site of large levee rehabilitation projects in which accurate characterization of the geologic environment has significant engineering importance. Results of the simulations predict that the average channel deposit dimensions are sensitive to the sedimentation scenario employed and are generally similar to those typically observed in fully meandering rivers. The results suggest that the channel aggradation rate influenced heavily the relative channel avulsion frequency during floodplain construction. Increased avulsion frequency equated to more numerous, yet smaller, channel deposits. Avulsion frequency and floodplain width affected the predicted fraction of the floodplain's cross-sectional width with subsurface channel deposits. The model for this study is simple and can be run in multiple iterations to produce probabilistic outputs. Such information can be used to predict the data collection density necessary to characterize the geotechnical properties of a project site.

Contents

Figures and Tables

Figures

Tables

Preface

This study was conducted using data collected as part of a series of investigations performed by the US Army Engineer Research and Development Center (ERDC) in support of various activities for the US Army Corps of Engineers (USACE), Fort Worth District.

The study was performed and documented by Dr. Brendan T. Yuill and Carla M. Roig-Silva of the Geotechnical Engineering and Geosciences Branch (GEGB), Geosciences and Structures Division (GSD), Geotechnical and Structures Laboratory (GSL), ERDC.

At the time the research was conducted, Danny W. Harrelson was Acting Chief, GEGB; Bartley P. Durst was Chief, GSD; Dr. William P. Grogan was Deputy Director, GSL; and Dr. David W. Pittman was Director, GSL.

At the time of publication, Chad Gartrell was chief, GEGB. COL Kevin J. Wilson was Commander, ERDC, and Dr. Jeffery P. Holland was Director.

Unit Conversion Factors

Multiply	By	To Obtain
acres	4046.873	square meters
feet	0.3048	meters
hectares	1.0 E+04	square meters
inches	0.0254	meters
miles (US statute)	1609.347	meters
square feet	0.09290304	square meters
square inches	6.4516 E-04	square meters
square miles	2.589998 E+06	square meters
square yards	0.8361274	square meters
yards	0.9144	meters

1 Introduction

The alluvial architecture of a river floodplain refers to the lithology and spatial distribution of the sedimentary facies that compose the floodplain's subsurface (Allen 1978). The character of the alluvial architecture plays an important role in determining the geotechnical properties within the floodplain, such as areas of high and low fluid seepage potential (Webb and Davis 1998; Willis and Tang 2010; Li and Caers 2011). Relatively coarse-grained architectural elements such as sand or gravel sedimentary deposits are porous and can be effective reservoirs of underground fluid such as water and hydrocarbons. Also, coarse-grained deposits have relatively high hydraulic conductivities and can be efficient seepage conduits. Because of these properties, it is necessary to understand the alluvial architecture of an area to properly construct and maintain engineering projects such as dams or levees that might be harmed by subsurface seepage (May and Schmitz 1996). Identifying floodplain areas with high seepage potential due to the underlying lithology (i.e., coarse-grained sediment deposits versus fine-grained sediment deposits) offers engineers the opportunity to reduce the probability that the project will be impacted by seepage.

The precise alluvial architecture of an individual floodplain is difficult to define because a large volume of floodplain material is involved, the architectural elements occur in a range of sizes, and most of the elements occur in the subsurface and are not directly measurable (Allen 1979; Koltermann and Gorelick 1996). However, the distribution of the sedimentary deposits composing a floodplain is primarily an artifact of the fundamental fluvial processes active within the floodplain through time (Blakey and Gubitosa 1984; Mohrig et al. 2000; Tye 2004; Peakall et al. 2007). Therefore identifying these processes, which are relatively well understood, and the manner in which they operate within a specific floodplain can show how sediment is locally distributed over time (Hajek and Wolinsky 2012).

For most fluvial systems, sediment exposed to fluvial flow is entrained dependent on (1) the relative force of the flow and (2) the relative resistance to entrainment presented by the sedimentary material, which typically increases with grain size and the cohesion of the material (Bagnold 1956; Leopold et al. 1964; Dietrich and Smith 1984). The balance of those two

factors and the pre-existing, external material composing the environment containing them (e.g., the underlying rock in an incising system) control much of the composition and organization of the river basin and its floodplain (Schumm 1968). In an actively building (aggrading) floodplain, the river channel is composed of sediment deposited by water flowing within the channel banks. The associated floodplain is composed primarily of sediment transported and deposited by unchannelized water, typically by overbank floodwater. These two types of flow and their associated sedimentation regimes are responsible for the first-order organization of the architecture for most aggrading floodplains (Fielding 1986; Paola 2000). Sediment transport capacity and competency, which set the amount and maximum grain size of sediment transport, are related exponentially to the magnitude of force exerted by flow. Generally, unchannelized flow occurring outside the channel within the floodplain produces lower tractive forces than that occurring within the channel system. This phenomenon creates a spatial disparity in relative sediment grain size within the drainage basin, as fine-grained sediment becomes deposited upon the floodplain surface and relatively coarse-grained sediment becomes deposited within the channel network itself (Allen 1974; Friend et al. 1979; Fielding 1986). As the floodplain aggrades, it becomes filled with two significantly different types of deposits: fine-grained floodplain ones composed of clays and silts and coarse-grained channel ones composed of sands and gravels (assuming the full range of grain sizes is present within the fluvial system). These two deposit types compose the alluvial architecture of interest for this study.

Examined were the fundamental geomorphic processes responsible for the distribution of coarse and fine sediment within a floodplain. A computational alluvial architecture model was employed to quantify how different processes (e.g., channel migration, avulsion, and sedimentation) might alter floodplain development. By identifying how these processes affect the alluvial architecture of the floodplain, it becomes possible to predict characteristics of the alluvial architecture, including those with engineering significance. Alluvial architecture-type models have been successful in identifying the influence of geomorphic parameters and processes for the distribution of coarse-grained sediment deposits relative to finer-grained deposits, but have not been widely used for applied studies outside of reservoir engineering and management applications (see North 1996; Bridge 2008; and Hajek and Wolinsky 2012 for eloquent reviews of alluvial architecture modeling). Alluvial architecture models explore how channel geometry, channel avulsion frequency, channel aggradation rate, and

uplift/subsidence affect the density of channel deposits within a floodplain cross section (Allen 1979; Bridge and Leeder 1979; Mackey and Bridge 1995; Leeder et al. 1996; Gross and Small 1998; Tornqvist and Bridge 2002; Jerolmack and Paola 2007; Willis and Tang 2010). They also help decipher the amount of dependence that the geomorphic parameters and processes they incorporate might have on each other, such as channel aggradation rate and avulsion frequency (Bryant et al. 1995; Heller and Paola 1996).

The objectives of this study were (1) to examine how the magnitude of specific geomorphic processes affects the alluvial architecture of a floodplain cross section with focus on the distribution of coarse sediment deposits (i.e., channel deposits) within the cross section and (2) to explore how the results of a computational alluvial architecture model can aid a geotechnical investigation for an engineering project. The model in this study was calibrated initially with data collected from a geological investigation in support of a levee engineering project, and the model's results were validated against the investigation's observations. An additional range of model input parameters, beyond that observed in the project area, was employed to better identify how fluctuation of these parameters can affect the modeled alluvial architecture elements that affect seepage.

2 Study Site

This study employs hydrologic, geologic, and topographic data collected from the upper Trinity River drainage basin near Dallas, Texas (Figure 1), and models the floodplain development of two cross sections within the study area (A and B in Figure 1). The bimodal distributions in topography differentiate the modern floodplain and the surrounding terraces. The river flows to the southeast. In Figure 1, a thick white line and a dashed white line illustrate the modern and the pre-realignment courses of the river, respectively. The small black crosses show the distribution and density of the geologic boring data collected in support of the levee projects. The thin, solid white lines show the locations of roads and bridges with associated boring data used by this study. These data were used to calibrate the model boundary conditions and initial parameters as well as to validate the model output. The Trinity River floodplain near Dallas is the site of multiple civil works levee construction and rehabilitation projects, with some dating to the early 20th century (Roig-Silva et al. 2010). The types and densities of geologic data collected for these projects illustrate the typical data demand, availability, and collection procedures common to modern infrastructure engineering projects.

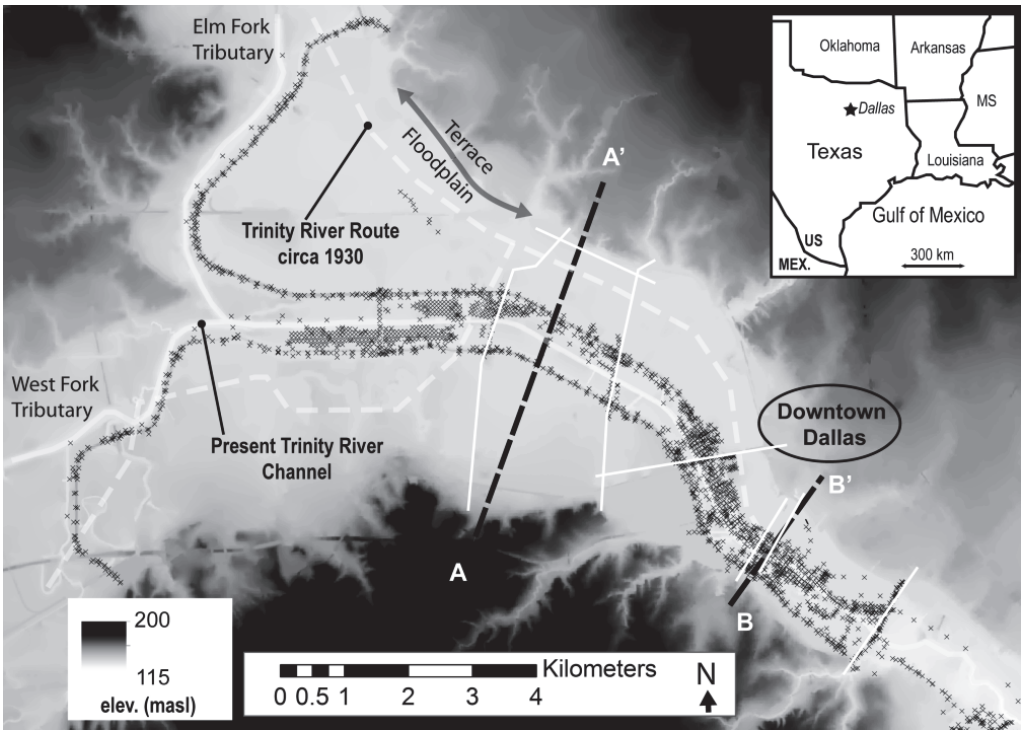

Figure 1. Map of the Trinity River floodplain near Dallas, Texas.

The river at Dallas drains an area of approximately 15,800 km^2. The city lies immediately downstream of the confluence of the Elm Fork and the West Fork of the Trinity River system. Three distinct quaternary terraces surrounding the modern floodplain have been identified. The lowest and youngest (formed 30 to 76 ka BP and called the Hickory Creek Terrace) lies 20 to 30 m above the modern floodplain at its location near Dallas (Ferring 1990). The north and south faces of the lowest terrace are well matched in this area and range from approximately 6 km apart at the upstream reach of the study area to about 1.5 km apart at the downstream extent. In the 1960s, municipal surface-water reservoirs were installed on both upstream tributaries of the Trinity River. Pre-1960 discharges for the 2-, 10-, and 50-year floods were 602, 1926, and 3943 m^3/s, respectively. Post-1960 discharges for the 2-, 10-, and 50-year floods have been reduced to 594, 1337, and 2105 m^3/s, respectively.

The modern Trinity River levee system was built in response to the initiation of the Dallas Floodway project in the 1920s. The project led to the eventual realignment of the Trinity River channel system to a parallel route approximately south of its natural course. A length of 36.4 km of 10-m-tall levees surrounds the current channel system, constraining it to a 0.5- to 1.0-km-wide floodplain. Before levee systems were in place, anecdotal evidence described large floods that inundated the full basin floor between the Hickory Creek terraces (Tompkins et al. 2010).

Geologic and geotechnical investigations conducted in support of the various Dallas Floodway projects obtained and synthesized more than 2000 geologic borings in the project area. The majority of the borings populate the area immediately surrounding the levee system, which approximates a third to half of the modern floodplain width. Additional boring data from highway and bridge locations, provided by the Texas Department of Transportation, were analyzed for this study to better characterize the full floodplain width. Boring data indicate that the bedrock (Cretaceous shale, chalk, and sandstone from the Eagle Ford and Austin Chalk formations) that underlies the modern floodplain sediments typically lies 5 to 20 m below the floodplain surface, dipping in the downstream (southeast) direction. In addition to the boring data, historic aerial imagery and topographic maps from 1891 to 1959 were obtained and geo-referenced to identify the river channel planform preceding its realignment. In general, the modern Trinity River appears to be of moderate sinuosity (1.5 to 1.7) with channel widths of 50 to 70 m and an average meander amplitude near 800 m.

3 Methods

Model description

This study employs a simple, computational model based on the two-dimensional Leeder, Allen, and Bridge (LAB) type alluvial architecture model (Allen 1974, 1978; Bridge and Leeder 1979; Mackey and Bridge 1992) that computes synthetic stratigraphy for a floodplain cross section. The model builds a floodplain cross section based on process-imitating rules derived from fluvial geomorphology and sedimentology that control the processes of floodplain sedimentation rate, avulsion frequency, and sediment compaction (i.e., consolidation). The cross section is built within a computational grid where the x-axis is the cross-valley distance and the y-axis is the vertical distance or depth. This type of cross section perspective is typical of that used to record and communicate geologic information for engineering applications. The computed stratigraphy differentiates between floodplain sediment deposited by channel processes (assumed to be relatively coarse, sandy sediment) and sediment deposited by overbank flooding (assumed to be relatively fine, silty, or clayey sediment). LAB models have been used in sedimentation research for both theoretical (Mackey and Bridge 1995; Heller and Paola 1996) and applied applications (Leeder et al. 1996; Bridge 1999; Bridge and Tye 2000; Karssenberg et al. 2001; Tornqvist and Bridge 2002). Typically, LAB models fix the dimensions of a channel deposit to a static mean value approximate to the average channel-belt width and the bank-full channel depth. In sedimentology research, channel-belt width often is estimated as the maximum amplitude of a meander loop (Allen 1974). The model employed in this study initially sets the channel deposit width to one bank-full channel width, but allows it to increase with time based on a defined lateral migration rate that is approximated as the bank erosion rate.

Figure 2 summarizes the model algorithm. The primary model components, in order of operation, are described below.

Boundary conditions

Cross-valley width (i.e., maximum floodplain width), base level topography, channel hydraulic geometry, initial channel location, and other initial conditions that define the model domain are set before each model

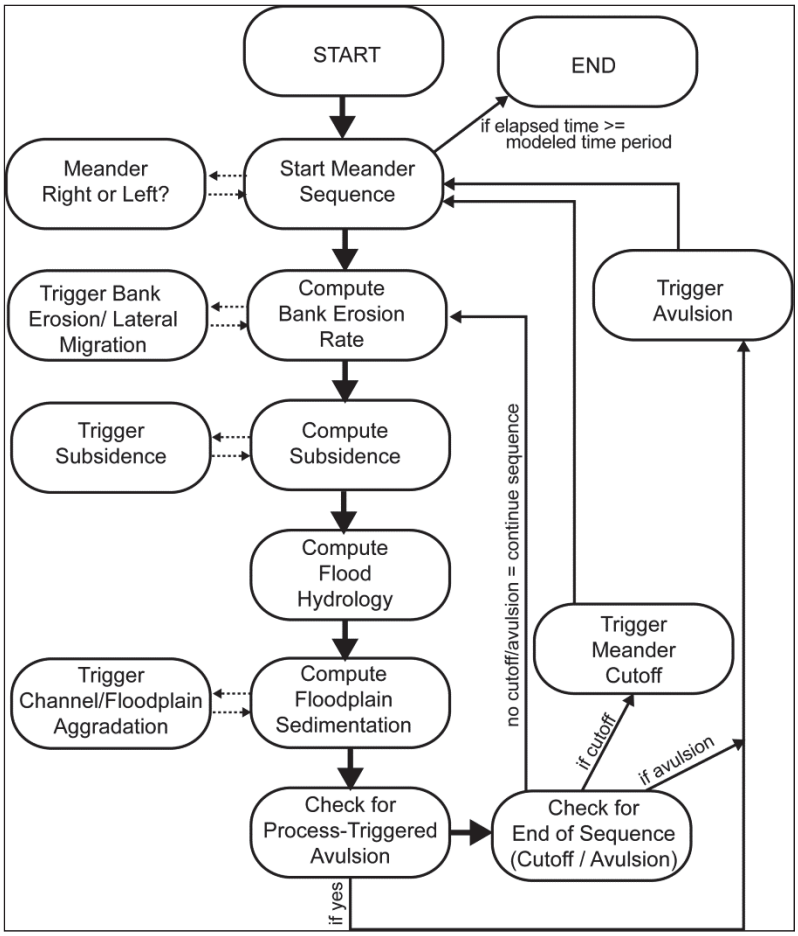

Figure 2. Diagram of the alluvial architecture model algorithm.

experiment and are defined. Channel dimensions can vary in time to accommodate induced changes in flow regime. For this study, the channel is unable to erode into the initial base-level topography, which simulates bedrock.

Meander sequence selection and lateral migration

The model begins by initiating a meander sequence (i.e., the formation of a meander loop with the assumption that the loop is bisected by the modeled cross section). The meander direction is selected randomly, and the meandering channel will migrate in this direction at a defined bank erosion rate shown in Figure 3. In the figure, Meander Amplitude (*MW*) is standardized by the average channel belt width (CBW_{AVG}). Bank erosion rates were approximated from observations reported in Tompkins et al. (2010). The channel will stop meandering in the selected direction under two conditions: a probability-based sequence termination or a process-based avulsion. The model laterally translates the channel location one grid

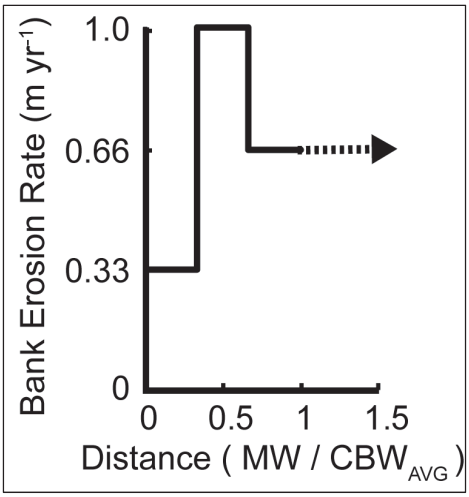

Figure 3. The estimated function between bank erosion rate and meander amplitude.

width, with elapsing time equal to the grid width divided by the bank erosion rate (which sets the time interval for the model step). Given uniform channel dimensions and surrounding lithology, the bank erosion rate often is correlated to the radius of curvature of the meander loop (Nanson and Hickin 1986). Because this model can resolve the landscape in only two dimensions, meander amplitude serves as a simple proxy for the radius of curvature and is used to adjust the channel migration rate based on the relative size of the meander in time.

The model deposits coarse-grained sediment within the cross-sectional area of the channel as it shifts in space. The continuous area of deposited coarse-grained sediment composes a channel deposit (Figure 4). Over a finite time period, the deposit width is a function of the channel width and the rate of lateral channel migration. The deposit depth is a function of the channel depth and the rate of channel aggradation. The development of a single channel deposit might include more than one meander sequence (i.e., the initiation, growth, and termination of one meander loop) and concludes due to a channel avulsion or the end of a model run.

Subsidence

The model simulates the effects of the compaction of floodplain sediments by subsiding the topographic surface. The subsidence rate is based on two criteria: the volume of compactable sediment per unit of floodplain width and the total volume of sediment above the compactable sediment (≈overburden weight). Sediment compaction is simulated by thinning the

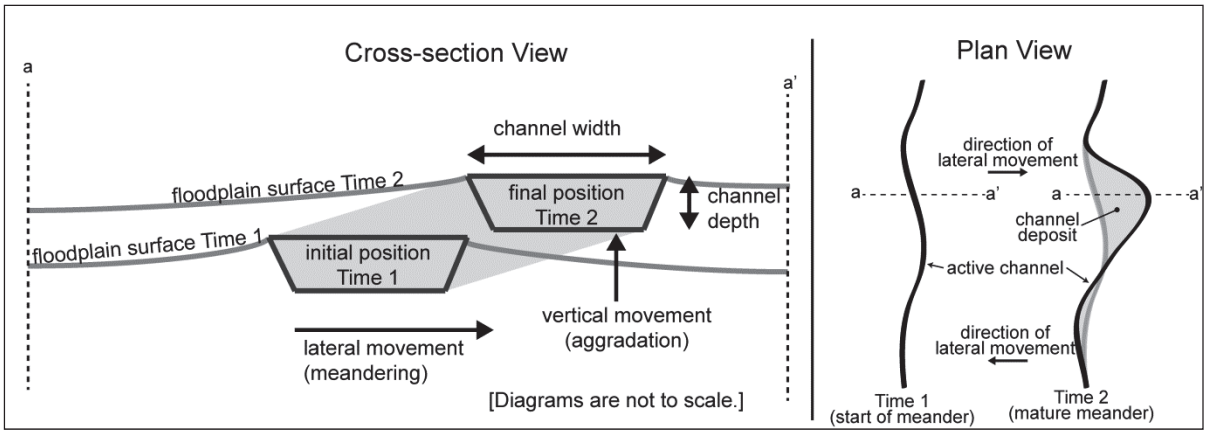

Figure 4. The controls of channel deposit (gray area) dimensions.

fine sediment deposits at the lowest elevation per unit floodplain width. This study sets the maximum possible subsidence rate to 0.5 mm/year, which approximates a typical rate for this process identified in literature (e.g., Milliman and Haq 1996).

Flood hydrology

The model computes a flood regime for each time interval of the model step. The magnitude of the regime is sampled randomly from a synthetic probability distribution (the model can employ either a Weibull or Log Pearson Type III distribution) calibrated by observed flood-frequency data. The maximum flood discharge for each time interval is used to estimate the probability of an avulsion or channel cutoff and the maximum lateral extent of floodplain deposition during that interval (Figure 5). The number of peak annual floods that exceed the bank-full discharge during each time interval is used to calculate the thickness of overbank sediment deposition for that interval.

Channel and floodplain sedimentation

The vertical distance the channel is aggraded during a single time interval is a linear function of the number of floods for that interval. The depth of floodplain sediment deposited over that interval for a unit of floodplain width (a_i) is a function of the magnitude of the channel aggradation (a_{CH}) and its relative horizontal, or cross-valley, distance from the channel margins (w_i), as given by:

$$a_i = a_{CH}\exp(-b\left(\frac{w_i}{w_{MAX}}\right)) \quad (1)$$

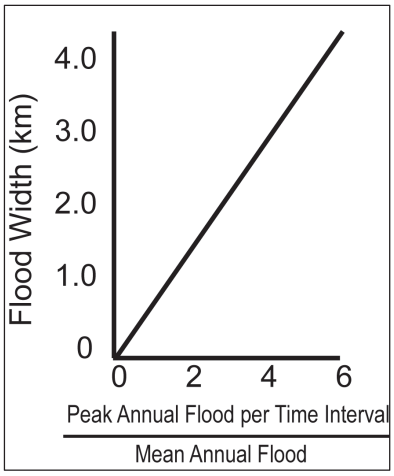

Figure 5. The relationship between relative flood discharge and flood width employed by the model.

where exponent b controls the rate of decrease in sedimentation with distance and w_{MAX} is the maximum lateral extent of the floodplain deposition (i.e., estimated flood extent). This equation has been commonly employed in LAB models. The value of the exponent b is difficult to calibrate for a specific site (Tornqvist and Bridge 2002); this study assumes a b value of 3.0, which is an approximate average value within the 0.35 to 10 range reported in published literature. The a_{CH} value associated with a single flood event was selected based on a model sensitivity analysis. The analysis identified the a_{CH} value that reliably reproduced the total floodplain aggradation computed from the geologic borings at each modeled cross section during the total period of analysis.

Process-based avulsions

For each time interval, the model computes the probability that a process-based avulsion will be triggered at the current channel location. The avulsion trigger is modified from the empirical relationship employed by Mackey and Bridge (1995) and is based on two ratios: (1) the maximum estimated flood discharge computed during that time interval divided by the estimated bank-full discharge and (2) the cross-valley slope computed during that time interval divided by the longitudinal channel slope. If both ratios exceed unity, it is assumed the conditions required for avulsion are present. An avulsion then is triggered based on the probability distribution defined in Figure 6, which equates increased probability with the degree of super elevation computed at the present channel location. In this study, super elevation is calculated as the height of the channel above the

minimum floodplain surface elevation. Field data (Mohrig et al. 2000; Jerolmack and Mohrig 2007) have shown that avulsion frequency increases rapidly at a super elevation of twice the bank-full channel depth (Figure 7). If triggered, the channel is relocated and inset at the nearest section of floodplain at the minimum surface elevation. In Figure 7, because the channel aggraded to a super elevation above 2, the channel bed is perched above the mean floodplain elevation. A levee breach in this situation could result in the evacuation of the full flow from its current course.

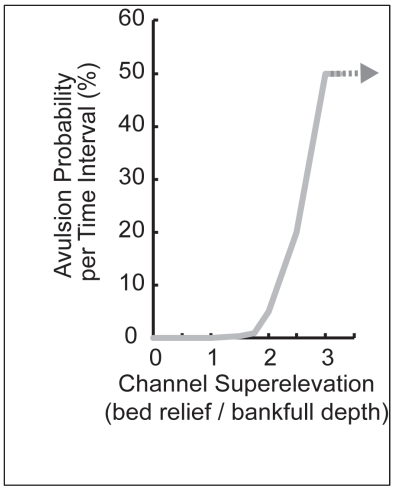

Figure 6. The probability a process-based avulsion will occur vs. channel super elevation per time interval.

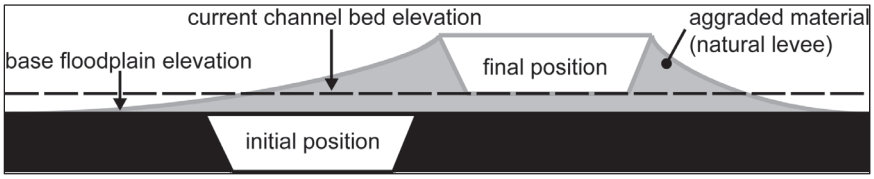

Figure 7. Diagram of a channel with a high probability of avulsion.

Channel cutoffs and probability-based avulsions

The probability that a modeled meander sequence will be terminated at the conclusion of each time interval is a function of the current meander loop's amplitude (Micheli and Larsen 2011), which is illustrated in Figure 8a. This probability distribution was computed to reproduce the observed range of meander sizes (sinuosity) in the modern upper Trinity River. The relative probability that the meander sequence will be terminated by a neck cutoff, chute cutoff, or avulsion is illustrated in Figure 8b. Typically, neck cutoffs do not occur until the meander loops approach a maximum probable amplitude.

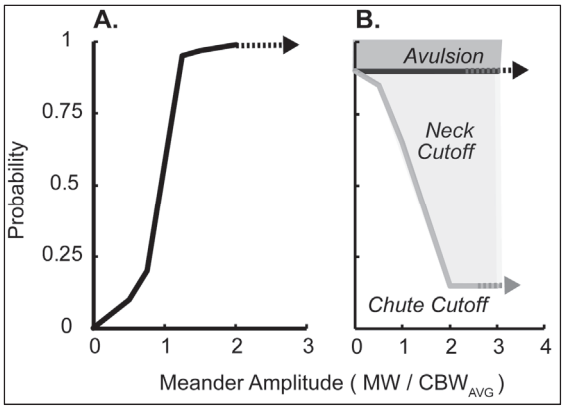

Figure 8. (A) The cumulative probability a meander sequence will terminate and (B) the probability a specific type of sequence termination will occur based on the meander's current amplitude relative to the average channel belt width.

Probability-based avulsions simulate those that occur upstream of the modeled cross section and are not influenced by the local environment. In this case, the post-avulsion location is selected randomly from any position along the lowest elevation level at the time the avulsion is triggered. For this study, the design probability for an upstream avulsion is 0.1% annually.

Description of experiments

Two cross sections (A and B in Figure 1) were modeled. Cross section A to A' (X-sec A) is located approximately 5 km upstream of cross section B to B' (X-sec B). X-sec A is 4.5 km wide, and the average depth of alluvial sediment above bedrock is about 12 m. X-sec B is 1.5 km wide, and the average depth of sediment is about 15 m. For both cross sections, the model's computational grid was set to produce a horizontal resolution of 10 m and a vertical resolution of 0.01 m. The bank-full channel dimensions were set at 3 m deep and 60 m wide. Five different scenarios were modeled at each cross section, producing 10 experiments (Table 1). The total period modeled was 11,000 years. It was assumed that the floodplain sediments had been deposited since the last sea-level low stand at the beginning of the Holocene (Ferring 1990). The modern (pre-realignment) cross-valley location of the channel along each channel cross section was selected to be the initial channel location for each model run. This ensures the model will predict at least one channel deposit at the cross-valley position observed during its engineered realignment.

Table 1. Summary of variables for the 10 experiments.

EXPERIMENT	X-SECTION	SCENARIO	
		sedimentation	initial topography
1	A	steady-state (ss)	uniform
2	A	climate change	uniform
3	A	ss x 2	uniform
4	A	steady-state	non-uniform
5	A	climate change	non-uniform
6	B	steady-state	uniform
7	B	climate change	uniform
8	B	ss x 2	uniform
9	B	steady-state	non-uniform
10	B	climate change	non-uniform

Experiments 1, 4, 6, and 9 employed steady-state channel aggradation rates of ≈ 4 and ≈ 3 mm per annual flood, exceeding bank-full for X-sec A and X-sec B, respectively, which were derived from the estimated total volume of the Holocene sediment at each location and the modeled time period. To simulate the effects of the climate change the region likely experienced during the modeled period, a variable channel aggradation rate was employed in Experiments 2 and 7 (Figure 9). The sedimentation rate was fit to the general regime described in Ferring (1990) for the upper Trinity River drainage system. In this scenario, aggradation rates were set as relatively high during wet periods and relatively low for dry periods. The temporally averaged channel aggradation rates for the climate change and the steady-state scenarios were the same. To replicate a shift in channel planform from a braided channel to a meandering channel during the channel change scenario, the channel width-to-depth ratio was set to evolve from 90:3 to 50:3. Experiments 3 and 8 explored the effect of increasing the channel aggradation rate two-fold relative to the steady-state scenario.

Experiments 4, 5, 9, and 10 were conducted using a non-uniform base level to simulate the effect of a more diverse initial topography at the beginning of each model run. This topography was estimated from boring data, which indicated that the channel initially was incised within a bedrock canyon approximately 10 m below the mean elevation of the contemporaneous floodplain (Roig-Silva et al. 2010).

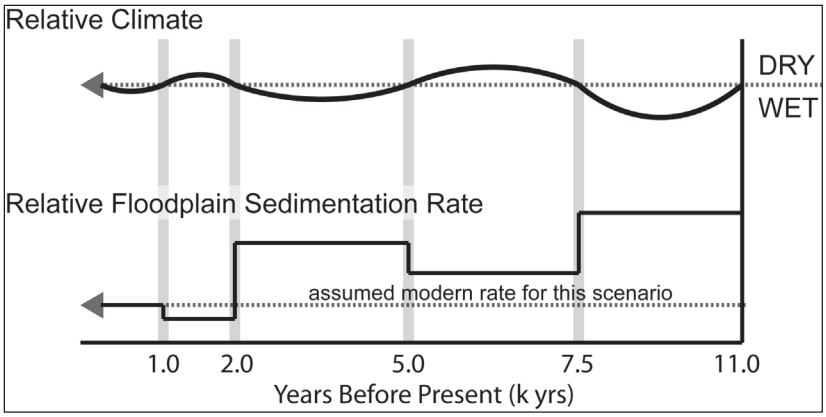

Figure 9. The relative climatology and sedimentation regime employed in the climate change scenario.

For the purposes of this report, Experiments 1 and 6 are considered the base case (i.e., the least complex scenarios) for X-sec A and X-sec B, respectively. Experiments 2 through 5 and 7 through 10 were conducted to explore how altering model parameters affects the model output.

The alluvial architecture model was run 100 times (simulating the construction of 100 cross sections) for each of the 10 experiments (i.e., two cross-section locations multiplied by five scenarios). Sensitivity analyses indicated 100 iterations were adequate to identify the average tendencies produced by the model.

4 Results

Computed deposit abundance and dimensions

Figure 10 shows an annotated example of a floodplain cross section at the conclusion of one model run from Experiment 1. The white lines in Figure 10 indicate the evolving position of the channel within the floodplain during the floodplain's development. The numbers indicate the elapsed model time in 100-year increments when the channel was at that position. In this example, five separate channel deposits were formed. Three of these deposits experienced some spatial overlap. Approximately 3.5 km of the 4.5 km cross-section width contained subsurface sand from a channel deposit. Channel deposits ranged from 1 to 3 channel depths (3 to 9 m) in thickness and 300 m to 1200 m in width. The combination of simultaneous lateral migration and vertical channel aggradation produced channel-deposit cross sections that slope upward in the direction of the channel migration. This phenomenon was observed in other studies predicting meandering-channel geometry (i.e., Bridge 1975; Gross and Small 1998) and is accentuated visually by the vertical exaggeration employed to illustrate a modeled cross section.

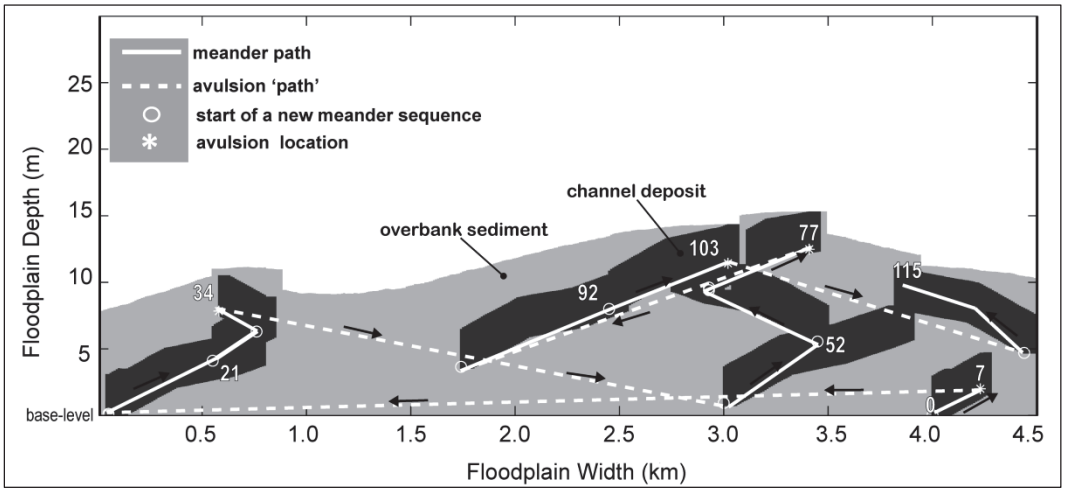

Figure 10. Example of a floodplain cross section computed for the base case of X-sec A (i.e., Experiment 1).

The different experimental scenarios produced significant variations within the distributions of computed channel deposit dimensions (Table 2). The distributions of the deposit widths computed during each experiment are illustrated in Figure 11. The experimental scenarios from X-sec A produced

higher maximum deposit widths; however, the scenarios from X-sec B routinely produced a larger proportion of relatively large width values. Deposit width values did not display a robust correlation with deposit thickness values. Figure 12 shows the relationship between width and thickness for individual deposits computed during Experiments 1, 4, and 6. In this figure, the widths of the observed meander belt (800 m), the incised bedrock channel in Experiment 4, and the total floodplain in Experiment 6 are shown for reference.

Table 2. Summary statistics for the deposit dimensions modeled in Experiments 1 through 10.

Exp #	Deposits per X-sec	DEPOSIT DIMENSIONS					
		Width (m)		Avg Thickness (m)		Max Thickness (m)	
		avg	*stdev*	*avg*	*stdev*	*avg*	*stdev*
1	4.2	837	334	5.3	1.4	7.7	2.3
2	4.9	772	325	5.1	1.4	7.3	2.3
3	6.8	649	234	5.2	1.3	7.7	2.2
4	4.3	796	288	5.4	1.8	7.8	3.1
5	4.9	699	261	5.8	2.3	7.8	3.2
6	3.0	919	337	7.0	2.0	9.5	3.1
7	3.5	842	324	6.6	2.0	8.8	3.1
8	4.3	793	316	7.0	2.2	10.1	3.5
9	3.3	808	336	6.5	2.3	9.1	3.6
10	3.6	757	317	6.6	2.3	8.7	3.3

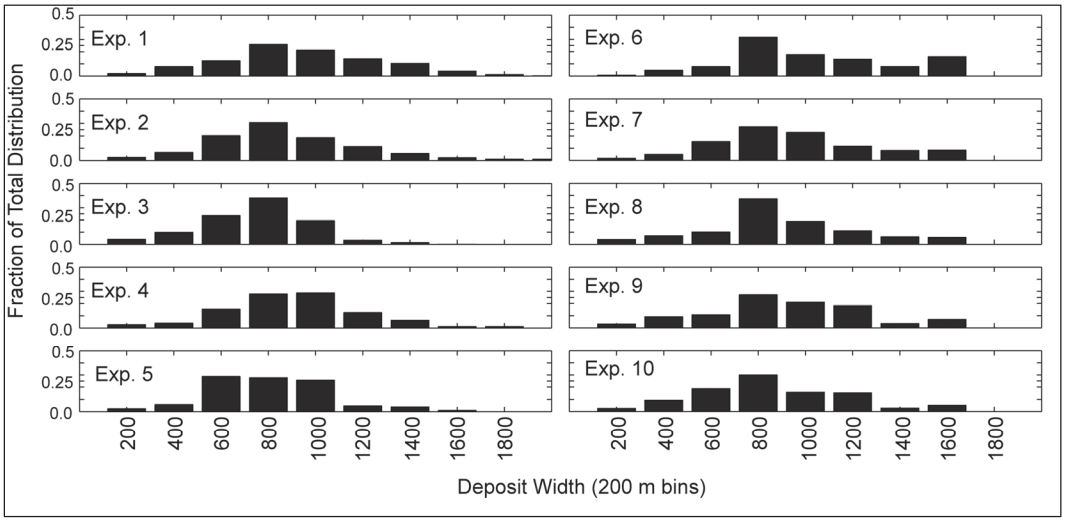

Figure 11. Histogram of the computed deposit widths for each experiment.

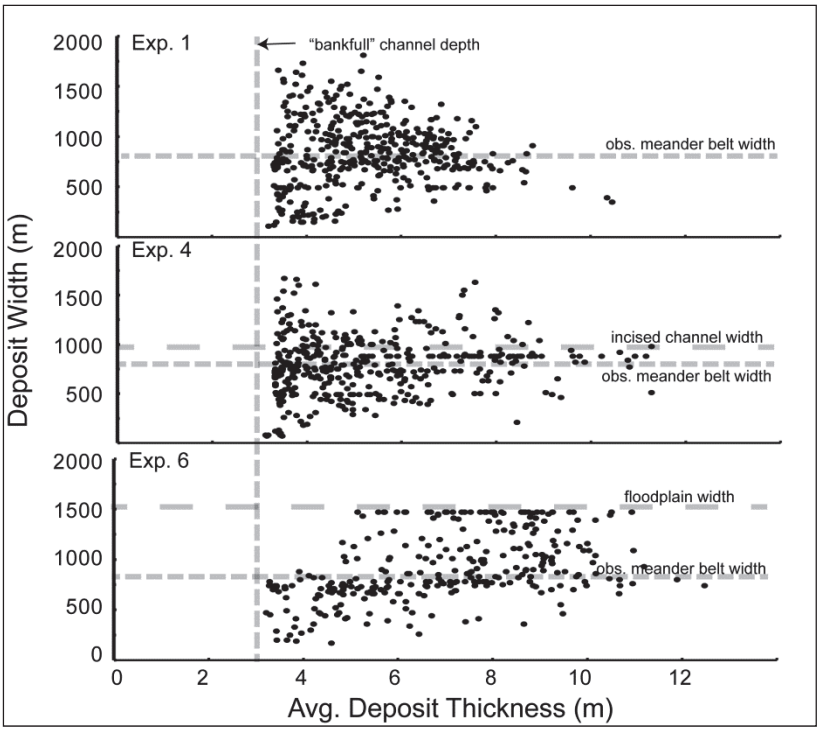

Figure 12. The relationship between deposit thickness and width for Experiments 1, 4, and 6.

The results from Experiment 1 represent the base case for X-sec A. The base case averaged 4.2 channel deposits per modeled cross section with an average deposit width of 837 m (Table 2). The average thickness of a channel deposit was 5.3 m, and the average maximum thickness per deposit was 7.7 m. The thickness of a channel deposit predominately depended on the frequency in which the channel reoccupied the same section of floodplain width (due to multiple cutoffs, which reset the channel location) during an inter-avulsion period. Experiment 6 represents the base case for X-sec B. For the two base cases, X-sec B contained a smaller average number of channel deposits (3) than X-sec A; however, the deposits were on average wider (919 m) and thicker (7 m).

The alternative scenarios, represented in Experiments 2 through 5 (X-sec A) and 7 through 10 (X-sec B), produced some fundamental differences in the floodplain architecture compared to that produced by the base case scenarios. Figure 13 shows cross sections computed from four of the alternative scenarios and illustrates these differences. The alternative scenarios typically increased the number of deposits and decreased the widths of deposits compared to the base case scenarios (Figure 14). Deposit thicknesses were decreased marginally during the climate change and the

doubled-sedimentation rate scenarios relative to the base case scenarios. Increasing the base-level complexity increased the deposit thickness in X-sec A and decreased it in X-sec B.

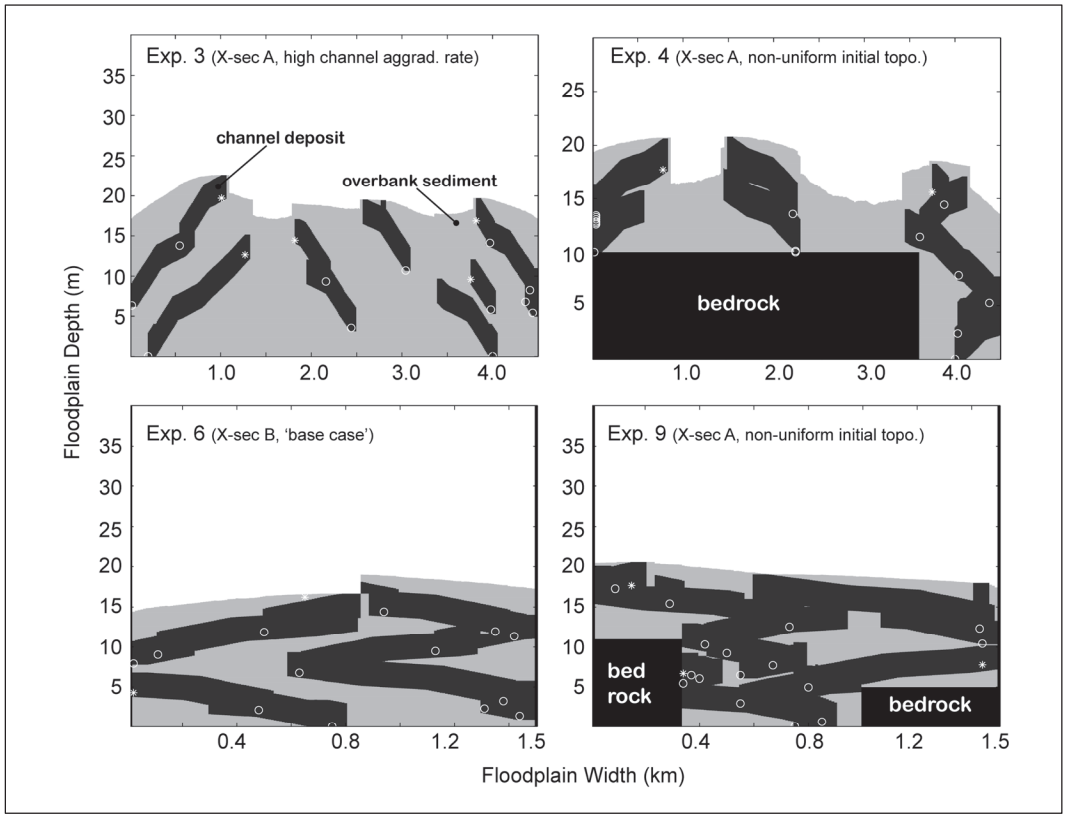

Figure 13. Example floodplain cross sections computed for four experiments. The figure uses the same symbology as that described in Figure 10. The plots for Experiments 4 and 9 display the initial bedrock topography employed for the non-uniform initial topography scenarios.

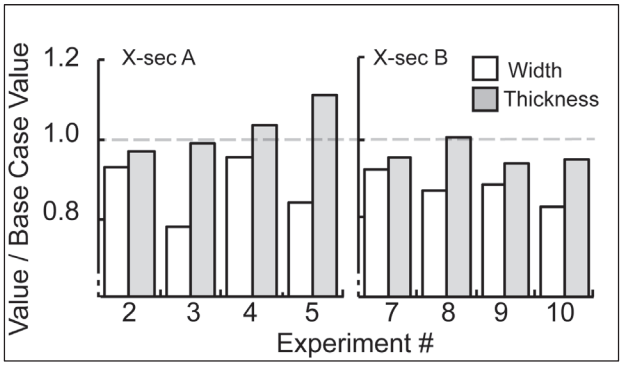

Figure 14. Average deposit dimensions for Experiments 2 through 5 and 7 through 10 relative to the base case values for X-sec A and X-sec B.

Avulsion frequency

Table 3 shows the frequency of process-based avulsions for each of the 10 experiments and compares those frequencies to the average frequency value computed for X-sec A and X-sec B. The average process-based avulsion frequency for X-sec A was greater than twice that of X-sec B (2.8 per model run vs. 1.2 per model run). Experiments 3 and 8, which included doubling the steady-state sedimentation rate, experienced a significantly higher avulsion frequency than the other experiments. Figure 15 shows the process-based avulsion frequency computed for each experiment was well correlated to both the average number of deposits per cross section (positive) and the average deposit dimensions (negative).

Table 3. The average and relative number of process-based avulsions per cross section for Experiments 1 through 10.

Exp #	Avulsions per X-sec (AV_i)	AV_i / AV_{AVG}
1	2.3	0.8
2	2.5	0.9
3	5.0	1.8
4	2.2	0.8
5	2.2	0.8
Avg for Exp 1 – 5 (AV_{AVG})		**2.8**
6	0.8	0.9
7	1.1	1.2
8	2.1	2.4
9	0.9	1.0
10	1.0	1.1
Avg for Exp 6 – 10 (AV_{AVG})		**1.2**

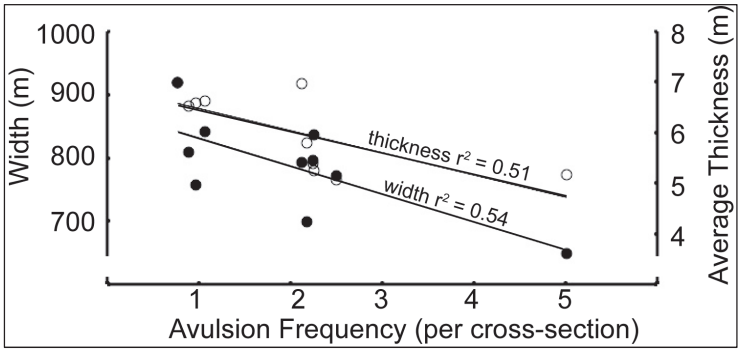

Figure 15. The relationship between the avulsion frequency and the average deposit dimensions for the 10 experiments. Open circles are thickness, and closed circles are widths.

Fraction of the floodplain width with underlying channel deposits

Figure 16 displays the fraction of the floodplain width computed to contain channel deposit sediment (i.e., subsurface sand) for the 100 model runs of each experiment. For the vast majority of model runs, more than half the floodplain width contained sand in the subsurface. Typically, 50 to 85% of the X-sec A width had subsurface sand, and 90 to 99% of the X-sec B width had subsurface sand. Figure 17 shows the average amount of sand (total sand thickness) per unit cross-section width (i.e., per row of the computational grid) and per unit cross-section depth (i.e., per column of the computational grid) for the two base cases. For Experiment 1, the average value of the total sand thickness ranged from 1 m at the middle of the cross section to 5 m at the cross-section margins. The total sand thickness per unit cross-section depth was greatest (average = 1580 m) at approximately 8 m above the initial cross-section base level. For Experiment 6, the total sand thickness per unit width was almost uniform along the entire cross section and averaged 8 m thick. The total sand thickness per unit cross-section depth was greatest (average = 1020 m) at approximately 5 m above the initial base level. Figure 18 is similar to Figure 17, except it displays data from the experiments with non-uniform initial topography and with steady-state sedimentation scenarios (i.e., Experiments 4 and 9). For these experiments, the spatial distributions of the total sand thicknesses were more variable than the base case scenarios. For Experiment 4, the average value of the total sand thickness per unit width typically ranged from 0 to 10 m; for Experiment 9, it ranged from 5 to 14 m. The segment of the floodplain cross sections that contained incised channels within the base level typically had the thickest subsurface sand. The total sand thickness per unit floodplain depth increased as the floodplain width increased at each depth interval.

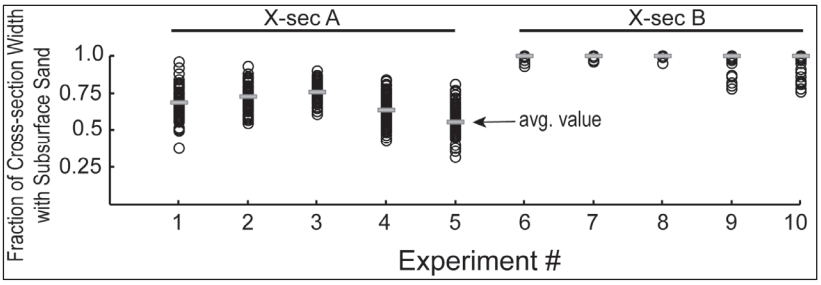

Figure 16. Percent of the floodplain width with subsurface sand under it.

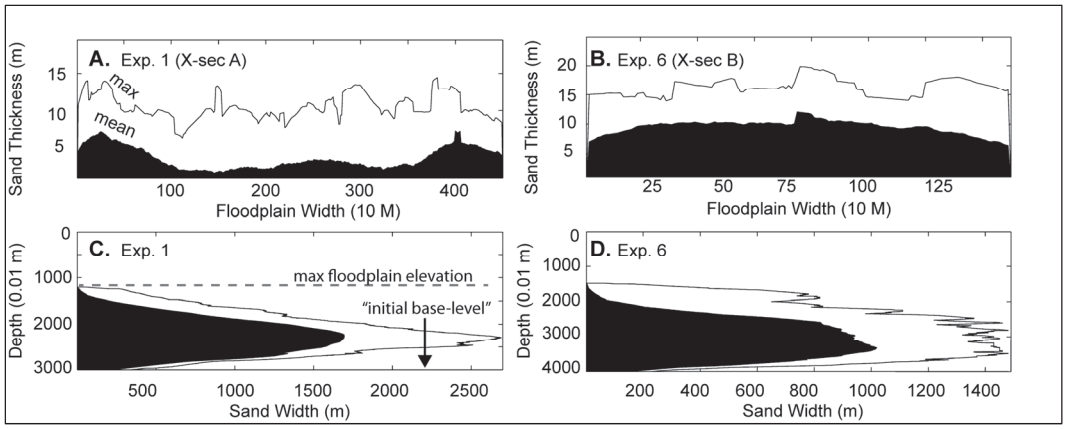

Figure 17. (A, B) Average values for the total sand thickness per unit floodplain width for the two base scenarios; (C, D) average width of sand within a floodplain per unit depth for the same two scenarios. Depth is in reference to an arbitrary datum set above the present-day topographic surface.

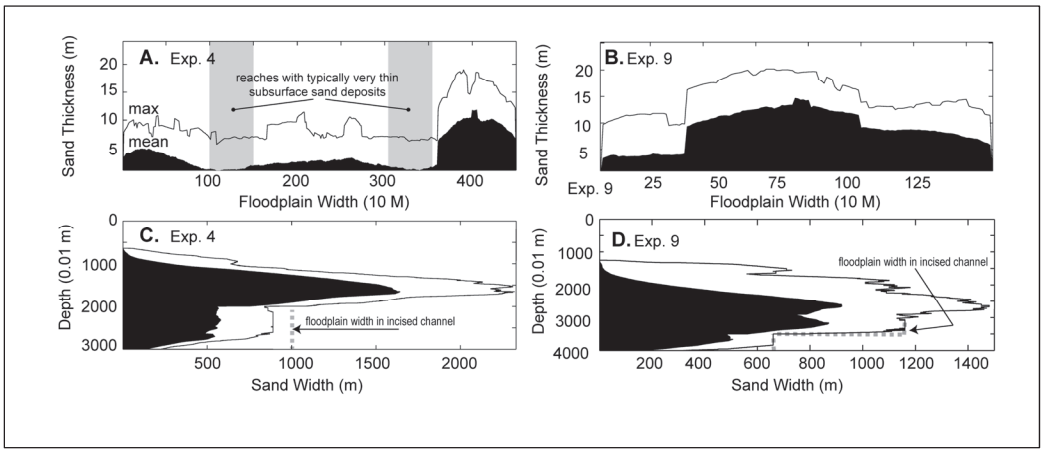

Figure 18. (A, B) Average values for the total sand thickness per unit floodplain width for Experiments 4 and 9; (C, D) average width of sand within a floodplain per unit depth for the same two scenarios. Depth is in reference to an arbitrary datum set above the present-day topographic surface.

5 Discussion

Interpretation of the results

Deposit dimensions

The base case experimental scenarios (Experiments 1 and 6) produced the widest channel deposits on average. For the other scenarios, the main factors that appeared to constrain channel deposit widths were the channel aggradation rate and the initial base-level topography. The influence of the channel aggradation rate was due to its positive impact on channel super elevation. In the employed model, super elevation was the primary trigger for process-based avulsions. Avulsions had the net effect of spatially disconnecting the locations of channel sediment deposition, ending the growth period of one deposit at one location and starting the growth period of another deposit at a new location. Experiments 3 and 8, which doubled the steady-state channel aggradation rate, had the highest avulsion frequencies, likely leading to their also having the largest number of deposits per cross section and the smallest deposit widths.

The scenarios that employed a non-uniform initial topography simulated floodplain aggradation on a base-level surface with an incised channel. The reduced valley width within the incised segment of the floodplain increased the probability that a valley wall would impede the modeled lateral migration of the channel. Limiting the lateral extent of the channel migration also would limit the lateral extent of the channel deposits. On average, this limitation would lead to smaller deposit widths within the computed architecture of the floodplains with incised channels than within the non-incised and, therefore, wider floodplains. For example, while the floodplain was aggrading within the incised channel in Experiments 4 and 5, the effective floodplain width was 1 km; therefore, the maximum possible deposit width during this period was 1 km.

Experiments conducted in X-sec B produced both fewer and larger average channel deposits than did experiments conducted in X-sec A. While the smaller floodplain width in X-sec B limited the maximum width values to below values observed in X-sec A (Figure 12), experiments in X-sec B routinely produced a higher percentage of very wide deposits (i.e., greater than 1000 m; Figure 11). This is likely because the model predicted more

uniform flooding across the relatively small floodplain in X-Sec B than in X-sec A (i.e., a flood inundated a larger fraction of the cross-section width in X-sec B than in X-sec A). More uniform flooding produces more uniform flood-dependent fine sediment deposition across the floodplain width. For experiments in X-sec B, the reduced cross-valley gradient in floodplain deposition produced less topographic relief and reduced the rate of channel super elevation relative to experiments in X-sec A. This resulted in a reduction of the process-based avulsion frequency by 50% relative to that observed in X-sec A.

Experiments in X-sec B computed higher deposit thicknesses than experiments in X-Sec A. This observation likely is correlated to the relative longevity of the growth period for these deposits due to the less frequent avulsions.

The modeled results show no significant relationship between channel deposit thickness and deposit width. A relationship between deposit thickness and width would be advantageous to engineers because the deposit-thickness data observed in boring logs could be used to extrapolate the associated deposit width. Figure 12 shows that deposit widths tend to cluster at distances influenced by the modeled boundary conditions such as the observed meander belt width, which was used to determine the probability that a meander cutoff or a probability-based avulsion would occur, and the floodplain widths, which limit the extent to which a deposit can grow. Deposit thickness showed little clustering at particular elevations above the minimum value (i.e., bank-full channel depth).

Deposit distribution

Theoretically, the fraction of a floodplain cross section that contains subsurface sand will rise on average due to increases in (1) the width of the sandy channel deposits and (2) the total number of deposits within the cross section. However, the model data show avulsion frequency, a primary control of these two influences, affects each influence in opposing ways. Increasing the avulsion frequency reduces the average deposit width but increases the overall number of deposits. This phenomenon likely reduces the sensitivity of the fractional value of the floodplain cross section containing subsurface sand to the different scenarios explored in this study.

For the experiments conducted in X-sec A, the fraction of the cross-section width without any subsurface sand deposits under it ranged from 25 to 45% on average, depending on the modeled scenario. Experiments 1 through 3 produced floodplain widths containing segments without any subsurface sand. The locations of these segments were not spatially consistent for every cross section simulated during the experiments. For the experiments conducted in X-sec A, the subsurface sand was consistently thinnest in two segments located at 1.0 to 1.5 km and 3.0 to 3.5 km along the cross-section width (measured using the south edge of the cross section as the origin). Experiments 4 and 5 produced very thin subsurface sand in these segments, including smaller sub-segments averaging zero thickness (Figure 18). The locations of these floodplain segments appear to result from compensatory channel-stacking processes inherent within the modeled processes. Compensatory stacking happens when channels change from positions of relatively high relief to positions of relatively low relief. During avulsions, areas remote from channel activity that have retained relatively low elevations due to low rates of sediment deposition are more likely to become new locations of the channel than areas close to the channel that were flooded frequently. Channel placement that selectively favors topographic lows has the net effect of leveling out the floodplain elevation in time. Evidence of compensatory stacking is common in certain sedimentary systems (Straub et al. 2009; Hajek et al. 2010; Hofmann et al. 2011). In this model, the location of the topographic low is set by (1) the channel location, (2) the cross-valley distance from the channel in which floodplain sediment can be readily deposited during floods, and (3) the total floodplain width. For the floodplain sedimentation regimes implemented within this model, the proximal topographic low (i.e., the closest cross-valley location at the lowest floodplain elevation) typically never was closer than 2 km from the active channel position. This promoted the buildup of channel deposit thicknesses, starting at the initial channel location and extending horizontally outward at approximate 2 km intervals. Past research on river avulsions in fluvial systems identified additional geomorphic factors that influence channel deposit stacking in other ways, such as the tendency of antecedent topography and gradients in soil erodibility to promote the reoccupation of paleochannels in time (e.g., Aslan et al. 2005; Jerolmack and Paola 2007). However, because of the simplicity of the model employed in this study, these factors were explicitly not considered.

Channel deposits did not appear stacked or clustered in X-sec B, where the total sand thickness was more evenly distributed along the cross-section

width relative to X-sec A (Figure 17b). The more uniform cross-valley deposition of floodplain sediments during floods in X-sec B prevented the buildup of large, cross-valley topographic gradients, which suppressed the activation of channel-stacking patterns within the sedimentary system.

Comparison with channel deposits observed

Figure 19 shows two geologic cross sections, which were interpreted from the available boring data for the same approximate locations as the modeled cross sections, X-sec A (19A) and X-sec B (19B). Assuming that (1) the sand facies identified in neighboring borings are both parts of the same deposit and that (2) the sand deposits were formed by channels oriented parallel to the longitudinal valley slope (NW to the SE), there appear to be three individual channel deposits per cross section. This might indicate at least two avulsions took place during floodplain development. These deposits have a similar average thickness of 5 m and a maximum thickness near 8 m, which is approximate to the mean thickness values predicted during the model experiments. The deposit widths appear larger in the cross section from Figure 19A than in the cross section from Figure 19B, which is in contrast to the values predicted by the computational model. The fraction of the floodplain widths underlain with subsurface sand (~ 75%) is approximately equal for both interpreted cross sections. The model computed that the floodplain near X-sec B would be almost completely underlain by subsurface sand. The interpreted cross section in Figure 19A does show channel deposits spatially distributed in the approximate pattern predicted by the model (i.e., located at the floodplain margins and within a central position). If the real-world alluvial architecture did not conform to the two assumptions stated above, the interpreted deposit dimensions likely would be overpredicted by the interpretation methodology.

Figure 20 illustrates the distribution of modeled width-to-thickness (w/t) deposit dimensions computed in this study in relation to observed values reported in literature. In addition, Figure 20 shows the range of deposit dimensions interpreted from Figure 19 and from Roig-Silva et al. (2010). Roig-Silva et al. (2010) reports 15 additional geologic cross sections interpreted from boring data collected from the fraction of the study area within the modern leveed floodplain. Typically, the w/t ratio for channel deposits decreases with the stability of the river channel (Gouw and Berendsen 2007), with high ratios associated with highly sinuous and

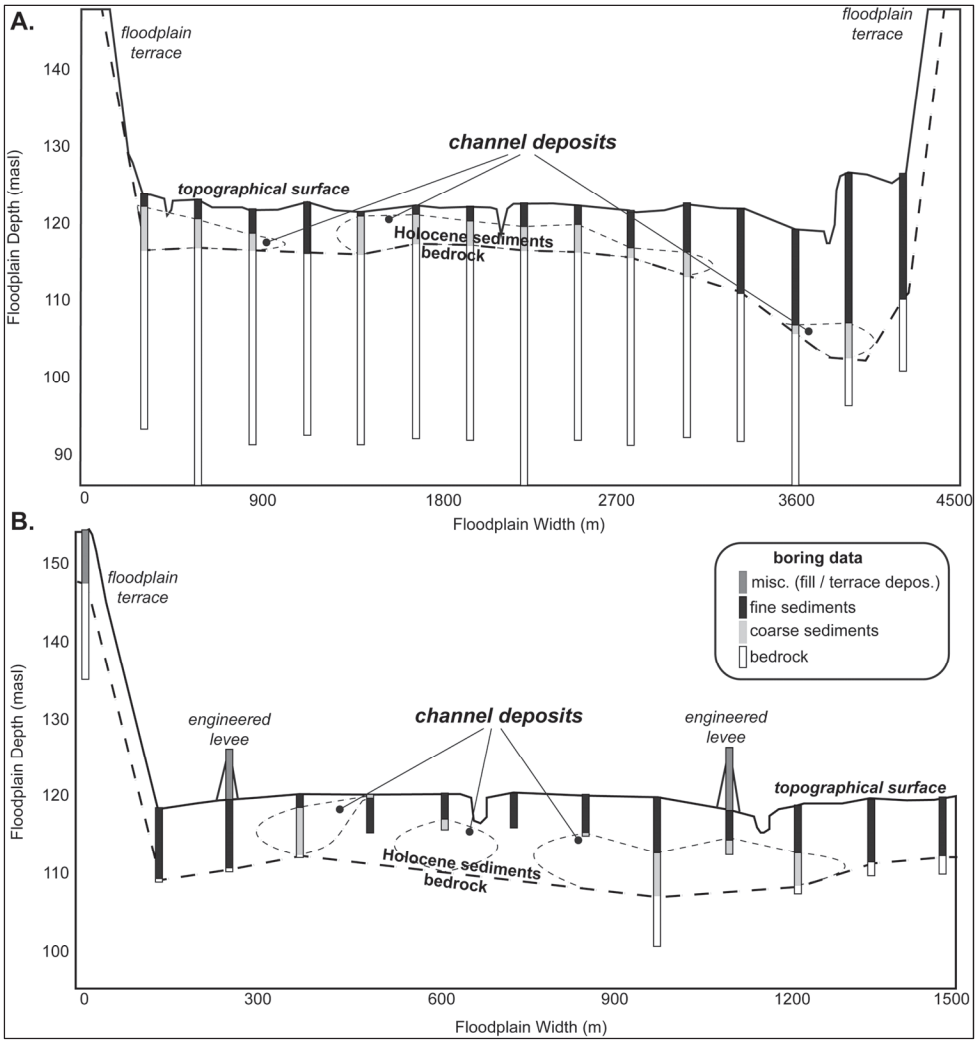

Figure 19. The alluvial architecture for the floodplain subsurface at locations approximate to (A) X-sec A and (B) X-sec B, as interpreted from available geologic boring data.

braided channels and low ratios associated with incised or straight channels. The modeled values are in general agreement with the data reported for fully meandering river channels (Fielding and Crane 1987; Gilbling 2006). Relative to the full range of values reported for meandering channels, the variations in the distribution of deposits values due to the different experimental scenarios examined in this study are small. This could indicate that the employed model is not as sensitive to the range of analyzed parameters as natural fluvial systems or that there are additional influential processes that the model does not consider. The distribution of deposit dimensions computed during an individual experiment is similar in size to the distribution of deposit dimensions measured along an individual river reach in large fluvial systems (Gouw and Berendsen 2007).

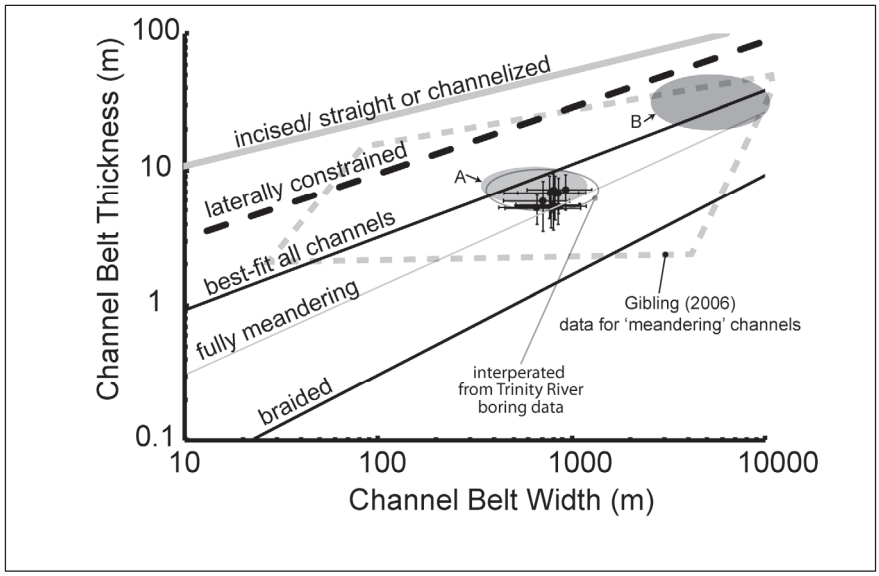

Figure 20. The modeled deposit dimensions relative to values observed in nature. The black circles are the average dimension values for the 10 experiments. The error bars represent the standard deviation of the values in each experiment. The exponential functions represented by the five trend lines were derived by Fielding and Crane (1987), from data from 45 published sources. The polygon bound by a dashed, gray line is the range of channel deposit dimensions found for meandering channels by Gibling (2006), who analyzed data from 1500 deposits. The shaded ovals approximately define the range of channel belt dimensions measured for two well-studied river systems: (A) the Linge River within the Rhine-Meuse Delta, Netherlands, and (B) the Lower Mississippi River, USA, as reported in Gouw and Brendsen (2007). The open gray oval illustrates the range of deposit dimensions estimated from geologic cross sections of the Upper Trinity River interpreted from the available boring data.

Engineering significance

The spatial distribution of subsurface sand deposits that influence regional gradients in soil porosity and hydraulic conductivity is of great importance in engineering projects such as dam and levee construction and maintenance. Typically, engineers characterize subsurface geotechnical properties by relying on geologic borings, cone penetrometer test (CPT) soundings, and geophysical surveys. However, the effectiveness of these methods depends on the balance between the overall size of the project area and the density at which the geotechnical properties are surveyed. It often is impossible to survey a project area at the resolution required to identify all the transitions between areas of high-seepage and low-seepage potential (i.e., sand deposit dimensions) due to capital and time limitations. Boring and CPT plans often are optimized by referencing geologic maps and historical imagery (i.e., a desk study); however, they often have spatial (e.g., small map scale) or temporal resolutions (e.g., imagery from few time

periods) that hinder the practical benefits. Geologic models such as those discussed in this report cannot identify specific sand deposit locations or their precise dimensions but, with minimal input data, can estimate the relative probability that an area contains sand deposits and the likely distribution of the sand deposit dimensions. This information is useful in assessing overall project risk and in directing resources to areas of enhanced seepage risk. For example, Figure 21 shows the probability that the width of a sand deposit will be effectively characterized using different boring, or CPT, spacing. In this example, it is assumed the deposit has an infinite length and that effective characterization requires the deposit to be penetrated or sampled twice (May and Schmitz 1996). For the predicted deposit sizes in the Trinity River project area, a 250-ft (76-m) boring spacing would reduce to an 80% chance that even the smallest deposits would be characterized while a 10,000-ft (3048-m) spacing would reduce the probability that the same range of deposit sizes would be characterized to 10%. Knowing the likely distribution of deposit sizes gives project managers the opportunity to optimize boring spacing by weighing the marginal costs associated with drilling additional borings against the desired probability of characterizing the seepage risk. Model data indicates a greater than 50% probability that the majority of subsurface channel deposits will be effectively characterized by a 3000-ft (914-m) boring spacing.

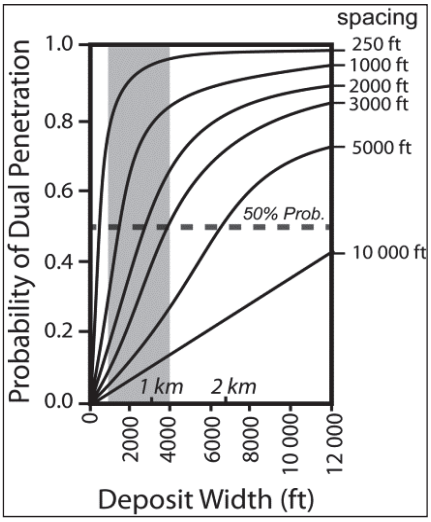

Figure 21. The probability a sand deposit will be penetrated twice at set boring spacings. The shaded area represents the estimated distribution of sand deposit sizes from this study. This figure is based on the statistical model in May and Schmitz (1996).

6 Conclusions

This study presents a simple computational model that predicts the distribution and size of sedimentary channel deposits within a floodplain cross section, based on a relatively small number of boundary conditions relating to geomorphic processes. Two cross sections were modeled for the Trinity River floodplain near Dallas. Five model scenarios were created by altering the model input parameters, and their results are reported. The dimensions of the floodplain width, the initial topography of the floodplain base level, and the channel aggradation rate were found to significantly affect the fraction of the floodplain width that contained subsurface sand deposits (Table 4). These parameters primarily influenced the distribution of subsurface sand by impacting the channel avulsion frequency during the floodplain construction. Avulsion frequency likely controlled the width and the total amount of the channel deposits within a floodplain cross section but in contrasting ways (i.e., increasing the total number of deposits typically decreased the deposit widths). This phenomenon made it difficult to identify how each experimental scenario explicitly affected the spatial distribution of subsurface sand.

Table 4. Average effect of the different experimental scenarios on model results relative to the base case results, unless otherwise stated. Values in italics indicate the scenario produced both increased and decreased values depending on the cross section location modeled.

Scenario	# Deposits	# Process Avulsions	Deposit Width	Deposit Thickness
X-sec B vs. X-sec A	-30%	-59%	10%	26%
Climate Change (*CC*)	16%	25%	-8%	-4%
Sediment Rate x 2	53%	148%	-18%	-1%
Non-Uniform (*NU*)	5%	-7%	-9%	*2%*
CC and *NU*	19%	*6%*	-17%	*2%*

The types of information provided by this modeling study are useful for engineers and planners working on projects where little is known about the subsurface environment, which is often the case. The model does not provide deterministic estimates of seepage magnitude or location; rather, it computes a distribution of possible frequencies and dimensions of seepage-prone areas based on a set of simple geomorphology-based rules.

While this information is simplistic, it can be valuable for a number of tasks. For example, interpretation of the model results suggests that relatively high channel aggradation rates and wide floodplains increase frequency of channel avulsions. Channel avulsions lead to smaller but more numerous and spatially distributed channel deposits. From an engineering perspective, a floodplain constructed under a fluvial regime with a high avulsion frequency would have a higher degree of uncertainty surrounding the location of possible sand-related seepage sites. The smaller channel deposit dimensions would decrease the probability that a single deposit fully traversed the subsurface area of a levee or a dam, a situation that puts that structure at greater risk of failure due to seepage.

Also, the identification of channel-stacking patterns that selectively favor the deposition of channel sediment into certain reaches of the floodplain width relative to others, such as those observed in the experimental scenarios taking place in X-sec A, could help to spatially partition the floodplain by seepage risk.

Additionally, the type of model employed in this study can help produce an informed estimate of the distribution of sand deposit dimensions. This information can be used to calculate the probability that a boring plan will effectively characterize the spatial distribution of geotechnical properties within a project area.

References

Allen, J. R. L. 1974. Studies in fluviatile sedimentation: Implications of pedogenic carbonate units, Lower Old Red Sandstone, Anglo-Welsh outcrop. *Geological Journal* 9:181-208.

_____. 1978. Studies in fluviatile sedimentation: An exploratory quantitative model for the architecture of avulsion-controlled alluvial suites. *Sedimentary Geology* 21:129-147.

_____. 1979. Studies in fluviatile sedimentation: An elementary geometrical model for the connectedness of avulsion-related channel sand bodies. *Sedimentary Geology* 24:253-267.

Aslan, A. S., W. J. Autin, and M. D. Blum. 2005. Causes of river avulsion: Insights from the late Holocene avulsion history of Mississippi River, USA. *Journal of Sedimentary Research* 75:650-664.

Bagnold, R. A. 1956. The flow of cohesionless grains in fluids. *Philosophical Transactions of the Royal Society* 249A:235-297.

Blakey, R. C., and R. Gubitosa. 1984. Controls of sandstone body geometry and architecture in the Chinle Formation (Upper Triassic), Colorado Plateau. *Sedimentary Geology* 38:51-86.

Bridge, J. S. 1975. Computer simulation of sedimentation in meandering streams. *Sedimentology* 22:3-43.

_____. 1999. Alluvial architecture of the Mississippi Valley: Predictions using a 3D simulation model. In *Floodplains: Interdisciplinary approaches,* ed. S. B. Marriott and J. Alexander, 163:269-278. Geological Society Special Publications.

_____. 2008. Numerical modeling of alluvial deposits: Recent developments. *Special Publication of the International Association of Sedimentology* 40:97-138.

Bridge, J. S., and M. R. Leeder. 1979. A simulation model of alluvial stratigraphy. *Sedimentology* 26:617-644.

Bridge, J. S., and R. S. Tye. 2000. Interpreting the dimensions of ancient fluvial channel bars, channels, and channel belts from the wire-logs and cores. *AAPG Bulletin* 84(8):1205-1228.

Bryant, M., P. Falk, and C. Paola. 1995. Experimental study of avulsion frequency and rate of deposition. *Geology* 23(4):365-368.

Dietrich, W. E., and J. D. Smith. 1984. Bed load transport in a river meander. *Water Resources Research* 20(10):1355-1380.

Ferring, C. R. 1990. Late quaternary geology and geoarchaeology of the Upper Trinity River drainage basin, Texas. *Unpublished Geological Society of America Field Trip #11 Guidebook.*

Fielding, C. R. 1986. Fluvial channel and overbank deposits from the Westphalian of the Durham coalfield, NE England. *Sedimentology* 33:119-140.

Fielding, C. R., and R. C. Crane. 1987. An application to statistical modeling to the prediction of hydrocarbon recovery factors in fluvial reservoir sequences. In *Recent developments in fluvial sedimentology*, ed. F. G. Ethridge, R. M. Flores, and M.D. Harvey, 39:321-327. SEPM special publication.

Friend, P. F., M. J. Slater, and R. C. Williams. 1979. Vertical and lateral building of river sandstone bodies, Ebro Basin, Spain. *Journal of the Geological Society of London* 136:39-46.

Gibling, M. R. 2006. Width and thickness of fluvial channel bodies and valley fills in the geological record: A literature compilation and classification. *Journal of Sedimentary Research* 76:731-770.

Gouw, M. J. P., and H. J. A. Berendsen. 2007. Variability of channel-belt dimensions and the consequences for alluvial architecture: Observations from the Holocene Rhine-Meuse Delta (the Netherlands) and the lower Mississippi Valley (USA). *Journal of Sedimentary Research* 77:124-138.

Gross, L. J., and M. J. Small. 1998. River and floodplain process simulation for subsurface characterization. *Water Resource Research* 34:2365-2376.

Hajek, E. A., P. L. Heller, and B. A. Sheets. 2010. Significance of channel-belt clustering in alluvial basins. *Geology* 38(6):535-538.

Hajek, E. A., and M. A. Wolinsky. 2012. Simplified process modeling of river avulsion and alluvial architecture: Connecting models and field data. *Sedimentary Geology* 257-260. http://dx.doi.org/10.1016/j.sedgeo.2011.09.005.

Heller, P. L., and C. Paola. 1996. Downstream changes in alluvial architecture: An exploration of controls on channel stacking patterns. *Journal of Sedimentary Research* 66(2):297-306.

Hofmann, M. H., A. Wroblewski, and R. Boyd. 2011. Mechanisms controlling the clustering of alluvial channels and the compensational stacking of cluster belts. *Journal of Sedimentary Research* 81:670-685.

Jerolmack, D. J., and D. Mohrig. 2007. Conditions for branching in depositional rivers. *Geology* 35(5):463-466.

Jerolmack, D. J., and C. Paola. 2007. Complexity in a cellular model of river avulsion. *Geomorphology* 91:259-270.

Karssenberg, D., T. E. Tornqvist, and J. S. Bridge. 2001. Conditioning a process-based model of sedimentary architecture to well data. *Journal of Sedimentary Research* 71(6):868-879.

Koltermann, C. E., and S. M. Gorelick. 1996. Heterogeneity in sedimentary deposits: A review of structure-imitating, process-imitating, and descriptive approaches. *Water Resources Research* 32(9):2617-2658.

Leeder, M. R., G. H. Mack, J. Peakall, and S. L. Salyards. 1996. First quantitative test of alluvial stratigraphic models: Southern Rio Grande rift, New Mexico. *Geology* 24(1):87-90.

Leopold, L. B., M. G. Wolman, and J. P. Miller. 1964. *Fluvial processes in geomorphology*. San Francisco: W.H. Freeman.

Li, H., and J. Caers. 2011. Geological modeling and history matching of multi-scale flow barriers in channelized reservoirs: Methodology and application. *Petroleum Geoscience* 17:17-34.

May, J. H., and D. W. Schmitz. 1996. Development of a predictive model for defining subsurface sand bodies. *Engineering Geology* 42:175-186.

Mackey, S. D., and J. S. Bridge. 1992. A revised FORTRAN program to simulate alluvial stratigraphy. *Computers and Geosciences* 18(2/3):119-181.

_____. 1995. Three-dimensional model of alluvial stratigraphy: Theory and application. *Journal of Sedimentary Research* B65(1):3-31.

Micheli, E. R., and E. W. Larsen. 2011. River channel cutoff dynamics, Sacramento River, California, USA. *River Research and Applications* 27:328-344.

Milliman, J. D., and B. U. Haq, ed. 1996. *Sea-level rise and coastal subsidence: Causes, consequences, and strategies*. Newton, MA: Kluwar Academic Publishing.

Mohrig, D., P. L. Heller, C. Paola, and W. J. Lyons. 2000. Interpreting avulsions process from ancient alluvial sequences: Guadalope-Matarranya system (northern Spain) and Wasatch Formation (western Colorado). *GSA Bulletin* 112:1787-1803.

Nanson, G. C., and E. J. Hickin. 1986. A statistical analysis of bank erosion and channel migration in western Canada. *GSA Bulletin* 97:497-504.

North, C. P. 1996. The prediction and modeling of subsurface fluvial stratigraphy. In *Advances in fluvial dynamics and stratigraphy,* ed. P. A. Carling and M. R. Dawson, 395-508. New York: John Wiley and Sons.

Paola, C. 2000. Quantitative models of sedimentary basin filling. *Sedimentology* 47:121-178.

Peakall, J., P. J. Ashworth, and J. L. Best. 2007. Meander-bend evolution, alluvial architecture, and the role of cohension in sinuous river channels: A flume study. *Journal of Sedimentary Research* 77:197-212.

Roig-Silva, C., A. R. Manning, B. D. Haugen, R. S. Olsen, J. B. Dunbar, D. W. Harrelson, and M. L. Pearson. 2010. *Geomorphic study of the Trinity River, Dallas, Texas*. TR 10-03-01.Vicksburg, MS: US Army Engineer Research and Development Center.

Schumm, S. A. 1968. Speculation concerning paleohydrologic controls of terrestrial sedimentation. *GSA Bulletin* 79(11):1573-1588.

Straub, K. M., C. Paola, D. Mohrig, M. A. Wolinsky, and T. George. 2009. Compensational stacking of channelized sedimentary deposits. *Journal of Sedimentary Research* 79:673-688.

Tompkins, M., G. Ajemian, A. Falzone, J. Thomas, P. Frank, and K. Winslow. 2010. 90 years of erosion and deposition on the Trinity River, Dallas, Texas. In *International Conference on Scour and Erosion 2010* (ICSE-5), 540-549.

Tornqvist, T. E., and J. S. Bridge. 2002. Spatial variation of overbank aggradation rate and its influence on avulsion frequency. *Sedimentology* 49:891-905.

Tye, R. S. 2004. Geomorphology: An approach to determining subsurface reservoir dimensions. *AAPG Bulletin* 8:1123-1147.

Webb, E. K., and J. M. Davis. 1998. Simulation of the spatial heterogeneity of geologic properties: An overview. In *Hydrogeologic models of sedimentary aquifers, SEPM concepts in hydrogeology and environmental geology,* ed. G. S. Fraser and J. M. Davis, 1:1-24.

Willis, B. J., and H. Tang. 2010. Three-dimensional connectivity of point-bar deposits. *Journal of Sedimentary Research* 80:440-454.

REPORT DOCUMENTATION PAGE

Form Approved
OMB No. 0704-0188

1. REPORT DATE *(DD-MM-YYYY)*	2. REPORT TYPE	3. DATES COVERED *(From - To)*
March 2013	Final	

4. TITLE AND SUBTITLE

A Computational Model to Simulate Groundwater Seepage Risk in Support of Geotechnical Investigations of Levee and Dam Projects

5a. CONTRACT NUMBER

5b. GRANT NUMBER

5c. PROGRAM ELEMENT NUMBER

6. AUTHOR(S)

Brendan T. Yuill and Carla M. Roig-Silva

5d. PROJECT NUMBER

5e. TASK NUMBER

5f. WORK UNIT NUMBER

7. PERFORMING ORGANIZATION NAME(S) AND ADDRESS(ES)

Geotechnical and Structures Laboratory
US Army Engineer Research and Development Center
3909 Halls Ferry Road
Vicksburg, MS 39180-6199

8. PERFORMING ORGANIZATION REPORT NUMBER

ERDC/GSL TR-13-5

9. SPONSORING / MONITORING AGENCY NAME(S) AND ADDRESS(ES)

US Army Corps of Engineers, Fort Worth District
809 Taylor Street 4A01
Fort Worth, TX 76102

10. SPONSOR/MONITOR'S ACRONYM(S)

USACE

11. SPONSOR/MONITOR'S REPORT NUMBER(S)

12. DISTRIBUTION / AVAILABILITY STATEMENT

Approved for public release; distribution is unlimited.

13. SUPPLEMENTARY NOTES

14. ABSTRACT

The amount and distribution of coarse-grained sediment relative to fine-grained sediment within a floodplain influences the floodplain's geotechnical properties, including the potential for groundwater seepage. Seepage is a primary driver of levee and dam failure, and understanding it is of paramount concern to water resource engineers and managers. This report documents the results of a computational modeling study that simulated alluvial floodplain construction by using simple geomorphic process-imitating rules. The model aggrades an alluvial floodplain, creating floodplain architecture by differentiating between sediment deposited by channel processes (coarse sediment) and sediment deposited by overbank flood processes (fine sediment). The evolution of two floodplain cross sections of the Trinity River near Dallas, Texas, is simulated under five scenarios. The study area is the site of large levee rehabilitation projects in which accurate characterization of the geologic environment has significant engineering importance. Results of the simulations predict that the average channel deposit dimensions are sensitive to the sedimentation scenario employed and are generally similar to those typically observed in fully meandering rivers. The results suggest that the channel aggradation rate influenced heavily the relative channel avulsion frequency during floodplain construction. Increased avulsion frequency equated to more numerous, yet smaller, channel deposits. Avulsion frequency and floodplain width affected the predicted fraction of the floodplain's cross-sectional width with subsurface channel deposits. The model for this study is simple and can be run in multiple iterations to produce probabilistic outputs. Such information can be used to predict the data collection density necessary to characterize the geotechnical properties of a project site.

15. SUBJECT TERMS

Computational model
Dams
Groundwater seepage
Levees

16. SECURITY CLASSIFICATION OF:			17. LIMITATION OF ABSTRACT	18. NUMBER OF PAGES	19a. NAME OF RESPONSIBLE PERSON
a. REPORT	b. ABSTRACT	c. THIS PAGE			19b. TELEPHONE NUMBER *(include area code)*
Unclassified	Unclassified	Unclassified		42	